Neural network simulation of original colors in Friedrich's Abbey Among Oak Trees featuring discoloured smalt

de Mecquenem, Clément; Eveno, Myriam; Alfeld, Matthias; Calligaro, Thomas; Laval, Eric; Mösl, Kristina; Reiche, Ina

DOI
10.1038/s40494-025-01953-y

Publication date
2025

Document Version
Final published version

Published in
npj Heritage Science

npj | heritage science

Article

https://doi.org/10.1038/s40494-025-01953-y

Neural network simulation of original colors in Friedrich's *Abbey Among Oak Trees* featuring discoloured smalt

Check for updates

Clément de Mecquenem[1,2], Myriam Eveno[3,4], Matthias Alfeld[5], Thomas Calligaro[1,2], Eric Laval[3], Kristina Mösl[6,7] & Ina Reiche[1] ✉

Artwork appearances change over time due to aging. Smalt, a blue cobalt-tinted glass pigment, deteriorates over time in oil paintings causing significant and irreversible color changes in many artworks. Virtual simulations can hypothesis original appearances while it remains a challenge for smalt-containing paintings. A novel procedure integrates non-invasive imaging methods, X-ray absorption near-edge structure (XANES), and machine learning to simulate the original colors of a smalt-containing discolored paintings. Macro-X-ray fluorescence provided elemental distribution, reflectance imaging spectroscopy captured color spectra of pigments and XANES informed cobalt speciation in cross sections. Friedrich's *Abbey Among Oak Trees* (1808-1810) containing smalt and artificially aged model systems were studied. Machine learning predicted the original hues based on XANES. The procedure allowed us to simulate the original, cooler and more vibrant colors of the painting. The innovative approach visualizes a possible original state of the smalt-containing artwork that can be adapted to other alteration phenomena.

Paintings may undergo various degradations or color changes over their lifetimes[1–5]. These alterations can be caused by accidents, be made on purpose, or occur naturally due to the aging of pictorial materials. Some of these modifications can be reversed through restoration processes, such as the yellowing of varnishes, which can be minimized by thinning it to reduce its visual impact[6]. However, others, such as the degradation of the smalt pigment, cannot be effectively restored, not only because the original color of the paint layer is often unknown but also because, even with this knowledge, it is impossible to reverse the chemical changes that have occurred. Moreover, overpainting the degraded areas with the original colors would not align with state-of-the-art restoration principles. Smalt is a potassium (K)-rich glass tinted blue by cobalt (Co), which was widely used as a pigment in oil paintings, murals, and polychromies from the 16th to 18th centuries[7,8]. The shade of this blue pigment varied based on grain thickness and Co concentration, which could range from 1–2% when used as a brightener to as much as 15% in painting applications. Typically, the Co content in smalt found in artworks ranged between 3 and 7%[9]. In addition to K and Co, smalt grains contained various other elements depending on the cobalt ores used for tinting, including arsenic (As), iron (Fe), nickel (Ni), and bismuth (Bi). However, smalt is known for its susceptibility to alteration in oil paintings. It leads to a transition from blue to a transparent hue that imparts a brownish tint to the paint layer due to the medium's color. This alteration occurs through ionic exchange between H^+ ions from the surrounding environment and K^+ ions from the glass grains. The leaching of K^+ ions results in several phenomena: they can react with the binder to form K soaps that migrate to the surface, creating a crust on the painting. Additionally, this leaching creates a charge deficit around Co^{2+} complexes, prompting their rearrangement within the glass matrix from tetrahedral to octahedral coordination. This structural change accounts for the pigment's loss of color in paintings, permanently altering the appearance of paintings[10–13].

As artworks are windows into our society at a particular time, their appearance significantly influences our understanding of the era or the art movement they represent. An alteration of their appearance can dramatically distort our perception of that time's artistic intentions and aesthetic values. Practically, it can also be a problem for restorers who must devise a suitable conservation strategy consistent with the significance and the state of preservation of the artwork[14]. Consequently, gaining insight into their original appearance by simulating the actual colors and nuances is crucial, as it allows for accurate knowledge and significance of the artwork within its

[1]Lab-BC, UAR 3506 CNRS / French Ministry of Culture / ChimieParistech - PSL University, Paris, France. [2]IPANEMA, UAR 3461 CNRS / French Ministry of Culture / UVSQ / MNHN, Saint-Aubin, France. [3]C2RMF, French Ministry of Culture, Paris, France. [4]PCMTH, IRCP UMR 8247 CNRS / Chimie Paristech - PSL University, Paris, France. [5]Delft University of Technology, Delft, The Netherlands. [6]Alte Nationalgalerie, Staatliche Museen zu Berlin-Stiftung Preußischer Kulturbesitz, Berlin, Deutschland. [7]Present address: Bayerisches Nationalmuseum, München, Deutschland. ✉e-mail: ina.reiche@culture.gouv.fr

societal and cultural context. Recent advances in color reconstruction have taken increasingly advantage of artificial intelligence (AI) techniques to address the complexities of degraded historical artworks. For example, convolutional neural networks have been employed to enhance image quality and restore faded colors by learning from extensive data sets of artwork, enabling more accurate virtual restorations[15]. In addition, generative adversarial networks (GANs) have been used to fill in missing areas of paintings by predicting lost details based on surrounding visual information, thus preserving the integrity of the original work[16]. These AI-driven methods improve the integration of scientific analysis with traditional restoration practices. In this context, we have developed a novel methodology that combines experimental data with machine learning (ML) tools to simulate the original appearance of paintings affected by smalt degradation. Although recent approaches primarily focus on the analysis of painting materials and the creation of imitations of pigment mixtures to estimate original colors[17–20], our method introduces a unique aspect by considering changes in the chemical composition of the painting. The altered state of smalt was evaluated using advanced techniques such as X-ray absorption near-edge structure spectroscopy (XANES)[21]. The procedure allowed the prediction of reflectance based on artificially aged model samples to estimate the contribution of smalt in pigment mixtures. This approach allows replacing the contribution of altered smalt in pigment mixtures by unaltered smalt and simulating the original color of the paint. Additionally, macro-X-ray fluorescence (MA-XRF) mapping and reflectance imaging spectroscopy (RIS) were carried out to identify and localize different pigments in paintings. The collected data are processed using machine learning methods such as clustering and artificial neural networks (ANN) to simulate the original color of the artwork. Our methodology was validated on artificially prepared and aged test samples and subsequently applied to Caspar David Friedrich's masterpiece, *Abbey among Oak Trees* (Alte Nationalgalerie, Staatliche Museen zu Berlin-Stiftung Preußischer Kulturbesitz, inv. no. NG 8/85), which contains altered smalt in numerous areas. Furthermore, our method is designed to be scalable across a wide range of paintings, achieved by developing a model trained on a dataset encompassing various degrees of smalt degradation. By integrating these advanced techniques, our methodology enables color predictions without requiring mock-ups for every pigment mixture, making it applicable to any painting.

Methods

Mock-up and test samples

For this study, several sets of smalt mock-up samples were prepared to reproduce smalt-containing paint layers. Deffner & Johann, a German supplier of materials, tools, and equipment for conservation and restoration, provided the smalt used to prepare those samples. This smalt smelt differs from the ancient one, without chemical impurities like As. Kremer smalt was also studied. To train the artificial neural network (ANN), we created four series of mock-up samples of smalt-based paints, differing in the nature of the binder used: linseed oil, walnut oil, siccative linseed oil and siccative walnut oil both with litharge as drying agent. These mock-ups consist of a layer of smalt mixed with each binder in a 1 g/1 g proportion. The mock-up samples were then artificially aged in a thermostatic oven at 70 °C in a vapor-saturated environment and without lighting[10]. One sample was not aged for each set of mock-up samples; the others were aged for different durations (Table 1). In contrast, the second set of test samples consisted of a mixture of smalt and hydrocerussite in a 1g/1g proportion, combined with cooked linseed oil. It was utilized for testing the simulation procedure as a proof of principle presented in the results of this article. The cooked linseed oil was prepared by heating it between 120 and 130° C for 4 hours (Table 1). The resulting paints were then spread on glass slides with a 90 μm thickness. For each preparation set, five mock-up samples were prepared to be artificially aged for different durations. Mock-up samples were prepared as thin sections of 30 μm thickness for the XANES spectroscopy at the Co K-edge.

Table 1 | Mock-up (set 1) and test sample (set 2) composition as well as their corresponding aging times

Set	Sample name	Composition	Aging time (h)
Set 1	LC0	Smalt in cooked linseed oil	0
Set 1	LC1		72
Set 1	LC2		192
Set 1	LC3		360
Set 1	LC4		552
Set 1	NC0	Smalt in cooked walnut oil	0
Set 1	NC1		72
Set 1	NC2		192
Set 1	NC3		360
Set 1	NC4		552
Set 1	LS0	Smalt in siccative linseed oil	0
Set 1	LS1		72
Set 1	LS2		192
Set 1	LS3		360
Set 1	LS4		552
Set 1	NS0	Smalt in siccative walnut oil	0
Set 1	NS1		72
Set 1	NS2		192
Set 1	NS3		360
Set 1	NS4		552
Set 2	SLW0	Smalt and hydrocerussite in equal mass proportions mixed in cooked linseed oil	0
Set 2	SLW1		10
Set 2	SLW2		24
Set 2	SLW3		48
Set 2	SLW4		240

Historical painting study

The painting *Abbey among Oak Trees* (1808-1810) by Caspar David Friedrich (Alte Nationalgalerie, Staatliche Museen zu Berlin-Stiftung Preußischer Kulturbesitz, inv. no. NG 8/85) was studied using non-invasive imaging techniques on site as well as on cross sections by means of scanning electron microscopy with energy-dispersive X-ray spectroscopy (SEM-EDX) in the laboratory and micro-XANES at the Co K-edge at synchrotron facilities (Supplementary Fig. 1).

Painting cross-sections and microscopic observations

Four micro-samples taken from the painting *Abbey among Oak Trees* were analyzed. The sample locations are indicated in the Supplementary Fig. 1. Microsamples were mounted as cross sections embedded in resin. Optical micrographs of these cross sections were obtained under different light sources in addition to SEM-EDX micrographs.

Optical microscopy

Cross sections were examined under different magnifications using a Nikon Eclipse LV100ND optical microscope, equipped with a Xenon lamp Power Supply XPS-100 and a Nikon DS-Ri1 camera, controlled by the NiSS-Element software. Three different illuminations were employed: bright field (BF) white light microscopy, which allowed for the examination of the sample surface, as well as two ultraviolet lightings: UV lighting fluorescence at 330-380 nm and blue fluorescence at 450-490 nm, which provided enhanced visualization of the paint layers and the smalt pigment.

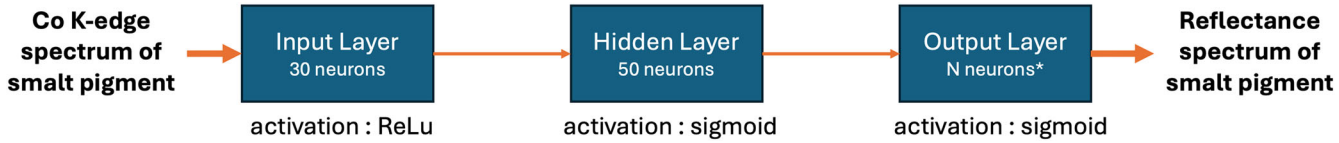

Fig. 1 | Architecture of the artificial neural network (ANN).

Scanning electron microscopy with energy-dispersive X-ray spectroscopy (SEM-EDX)

Quantitative elemental analysis and elemental mapping were performed using a JEOL 7800F scanning electron microscope equipped with two Bruker AXS 6|30 energy-dispersive X-ray detectors. To prevent charge accumulation, non-conductive samples were coated with platinum. The operational parameters included an acceleration voltage of 15 kV, a beam current of 3.6 nA, and a chamber pressure below 100 Pa. All spectra were processed using the Bruker Quantax Duo 400 analytical platform (Esprit software). Quantitative analysis for elemental ratios was determined with an internal reference and the results were expressed as oxide percentages.

X-ray absorption near edge structure spectroscopy (XANES) at the *Co* K-edge

The *Co* K-edge XANES spectra were recorded at the European synchrotron radiation facility (ESRF) on the ID21 beamline[22,23] and at the SOLEIL synchrotron radiation facility on the PUMA beamline[24,25]. At the PUMA beamline, the X-ray source is equipped with a Wiggler W164.2 mm × 20 periods, B = 1.8 T, medium section. The energy of the beam is selected by a double crystal monochromator (DCM) Si111 in the range of 4 to 20 keV and Si220 in the range of 20 to 60 keV. The beamline can provide a beam with a spot size of $5 \times 5\ \mu m^2$ at the *Co* K-edge. Spectra were acquired in fluorescence mode within an energy range of 7670 eV to 8000 eV in 0.5 eV increments and a counting time of 2s. At the ID21 beamline, the X-ray source is a 4.8 m long low-beta straight section and is equipped with three 1.6 m long undulators: two with a 42 mm period (U42) and one with a 32 mm period (U32). The U42 elements deliver maximum X-ray intensity in the energy range of 2–6 keV, while the U32 device covers the energy range of 6–9.2 keV. The energy of the beam is selected by a fixed-exit double crystal monochromator with a Si(111) ($\Delta E/E \sim 10 - 4$) or Si(222) ($\Delta E/E \sim 9.10{-}5$). The beamline could provide a beam with a spot size of $0.5 \times 0.7\ \mu m^2$ at the *Co* K-edge. Spectra were acquired under vacuum in fluorescence mode within an energy range of 7670 eV to 8050 eV in 0.5 eV increments.

Energy values were calibrated using reference data and known absorption energies. The data processing and spectra evaluation, such as auto-absorption correction, background correction and normalization, were completed using PyMca software[26].

2D Macro X-ray fluorescence mapping (MA-XRF)

Scanning X-ray fluorescence imaging of the painting was carried out using a prototype MA-XRF equipment integrating a Mo-based X-ray generator (ROENTEC X1 generator, RTW MCB 50–0.6, 50 kV, 1 mA max) operated at 45 KV, 0.5 mA with a 1 mm collimator producing a 1 mm beam spot on the painting[27]. XRF spectra were collected using a silicon drift detector (70-mm^2 AMPTEK X123 integrating a 512 channel MCA) placed at a 15 mm distance from the painting surface. A motorized stage measuring 600 mm x 500 mm (ZABER X-LRQ and A-LST) allowed the acquisition of the elemental maps with a step size of 1 mm and a 100 ms dwell time. The painting was too large to be acquired in a single scan, and thus, sixteen scans covering about 550 mm x 300 mm were taken, 5 h each, which were stitched together using DataHandlerP[28].

Reflectance imaging spectroscopy (RIS)

Data of the painting was acquired using a SPECIM IQ RIS camera, covering a spectral range from 400 to 1000 nm, with a spectral resolution of 3 nm (204 channels). Two ARRILITE 750 Plus illuminated the painting with 3200 *K* bubs at 50° of the surface layer. The camera was operated using an integration time of 100 ms. The datasets were calibrated using a ColorChecker Passport MSCCPP-B. The painting was too large to be acquired in a single scan, and thus, sixteen scans were taken and later stitched together using DataHandlerP[28]. The datasets were scaled to match the resolution of the MA-XRF scans, resulting in datasets of 960 × 1380 pixels.

Data of the mock-up samples was acquired using a HySpex1600 RIS camera with a resolution of 17 pixels per mm[29]. The spectral range extends from 416 to 992 nm and has 80 bands. The center of the bands is spaced from each other by 7.29 nm.

Artificial neural network (ANN) structure and training

The architecture of the developed ANN is given in Fig. 1.

The architecture consists of three layers: an input, a hidden, and an output layer. Each layer is described below:

Input Layer:

The input layer receives the *Co* K-edge XANES spectrum of the smalt pigment.

Neurons: 30 neurons.

Activation Function: ReLU (Rectified Linear Unit).

Purpose: To process and pass the input features to the next layer, introducing non-linearity to the model.

Hidden Layer:

This intermediate layer processes the data from the input layer to extract relevant features.

Neurons: 50 neurons.

Activation Function: Sigmoid.

Purpose: To capture complex patterns in the input data, enabling the network to learn intricate relationships between the *Co* K-edge XANES spectrum and the reflectance spectrum.

Output Layer:

The output layer generates the final predictions, which correspond to the reflectance spectrum of the smalt pigment.

Neurons: N neurons (the exact number depends on the specific requirements of the reflectance spectrum output).

Activation Function: Sigmoid.

Each neuron corresponds to a specific part of the spectrum to produce the reflectance spectrum values.

The neural network (NN) employs a straightforward feedforward architecture. The ReLU activation is defined as:

$$\mathrm{ReLU}(x) = \max(0, x) \tag{1}$$

in the input layer helps in dealing with non-linearity, while the sigmoid activation functions are defined as:

$$\sigma(x) = \frac{1}{1 + e^{-x}} \tag{2}$$

In the hidden and output layers, ensure that the outputs are within a [0,1] range, which is suitable to represent the spectrum values. This design allows the network to effectively learn the transformation from the *Co* K-edge spectrum to the reflectance spectrum of the smalt pigment.

The training of the model was performed with XANES spectra at the *Co* K-edge measured on mock-ups containing only smalt and binders as well as the reflectance spectra of the associated mock-ups. In total, 191 pairs

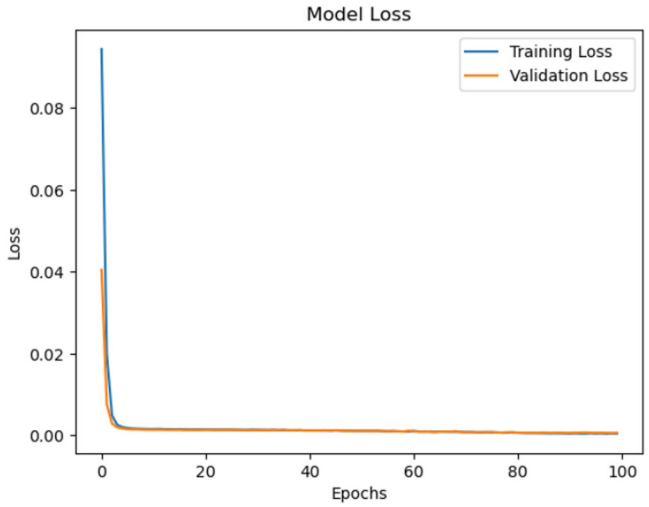

Fig. 2 | Plot of the training loss and validation loss in function of the number of epochs during the training of the ANN

of *Co* K-edge XANES spectra (Supplementary Figures 2–13) and reflectance spectra were used (Supplementary Figures 14–17). This data set was divided into two with an 80/20 ratio to create training and validation sets.

The training process for the NN was carried out using the Adam optimizer, which was selected for its efficiency and ability to dynamically adapt the learning rate. The learning rate was set to 0.01 to ensure a balanced pace of learning. The model was trained using the Mean Squared Error (MSE) loss function. It is suitable for our regression task as it measures the average squared differences between the predicted and actual values. We used a batch size of 32, iterating throughout the training dataset in small batches to stabilize and accelerate convergence. The training was carried out over a predefined number of epochs, during which the model parameters were iteratively adjusted to minimize the loss. Additionally, we monitored the validation loss at the end of each epoch to assess the model's performance on unseen data and to guard against overfitting. The NN performance was evaluated using both training and validation datasets to ensure a comprehensive assessment of its predictive capabilities. The loss curve for the training set demonstrated a steady decrease throughout the training process, indicating effective learning and improved fit of the model to the training data. Similarly, the validation loss curve initially followed a downward trend, reflecting good generalization to unseen data. However, after a certain number of epochs (around fifty), the validation loss plateaued and started to be higher than the training loss, suggesting the onset of overfitting. That's why we limit our training to fifty epochs to avoid overfitting. With these parameters, we obtain an average error of 0.0011 on the training set and 0.0011 on the test set (Fig. 2).

Procedure for the color simulation

The developed procedure, which is a Python code, involves several steps. It beginns with comprehensive data acquisitions and processing. Four series of mock-up samples and one series of test samples were created and artificially aged for different durations (Table 1). These series mimic a simple smalt-binder paint layer with varying types of oil binders to create a robust database reflecting the evolution of *Co* K-edge XANES spectra (Supplementary Figures 2–13) and the reflectance spectra of smalt as a function of the alteration state of the pigment (Supplementary Figures 14–17). The fifth series (test samples SLW0-4) was created by mixing smalt and lead white with cooked linseed oil to test the methodology developed on a simple and controlled example as a proof of principle (Table 1). In parallel, RIS and MA-XRF were employed to collect in-situ detailed spectral and elemental data of the painting *Abbey among the Oak Trees* by Caspar David Friedrich. These methods were complemented by *Co* K-edge XANES profiles performed on the micro-samples of the painting to evaluate the alteration state of smalt. Subsequently, the RIS and XRF data were stitched and fused to create a consistent dataset that combines spectral and elemental information, essential for analyzing the materials and their spatial distribution in the painting.

Following data acquisition and processing, the data undergoes clusterization using unsupervised ML techniques in the form of Principal Component Analysis (PCA) followed by k-means clustering as explained later in the article. This clustering process is used to separate areas within the painting containing different mixtures of pigments, and the analysis of these clusters allows for the identification of smalt-containing regions.

Furthermore, supervised learning techniques, specifically ANN previously trained on the mock-up data, are employed to simulate the reflectance spectrum of smalt as it appears today. This simulation utilizes the *Co* K-edge XANES spectra measured on micro-samples from the painting, incorporating the *Co* coordination environment of the pigment to estimate its original color. A pigment unmixing process is conducted for each cluster where smalt is identified. The unmixing is based on the simulated reflectance spectrum of altered smalt and the known reflectance spectra of other pigments mixed with smalt in the clusters. This process, which employs a simplified Kubelka-Munk model to model the interaction of light with the pigment mixtures[30–32], determines the contribution of each pigment to the overall reflectance spectrum. Finally, the reflectance spectra of the clusters are reconstructed using the spectral contributions of the pigments calculated previously, replacing the reflectance spectrum of altered smalt with the unaltered one. This provides a comprehensive spectral profile of the artwork as it may initially appear. Utilizing the reconstructed reflectance spectra of the clusters, a digital simulation of the original painting's appearance was created, offering a visual representation of the artwork. The scheme presented in Fig. 3 summarizes all the steps of the procedure.

Results

Proof of principle on test samples

The developed procedure was first tested on the test samples made of a mixture of smalt and lead white described in Table 1, before being applied to a historical painting.

After the measurements of the reflectance spectra of the test samples, the L*a*b* (CIELAB) values were calculated (Supplementary Fig. 18 and Supplementary Table 1). They show that the lightness (L*) tends to decrease (from 64.68 for the unaged sample to 41.84 for the most aged on) as the aging time increases. The b* value representing the yellow/blue coordinate is increasing (from -13.73 for the unaged sample to 6.84 for the most aged one). It demonstrates the darkening of the sample and the shift from a blue to a yellow tone with the aging time. Then, the mean XANES spectrum measured at the *Co* K-edge for each test sample shows that they change significantly with aging time (Fig. 4A). As aging progresses, the intensity of the white line, centered around 7.745 keV, increases and becomes sharper. Concurrently, the intensity of the pre-edge peak, centered around 7.728 keV, decreases with aging time. This indicates a change in the coordination environment of Co^{2+} ions during the aging process.

For simulating the original color of the sample presenting unaged smalt, it is necessary to determine the reflectance spectrum of the smalt pigment in its state in the aged sample mixture. The ANN mentioned above can simulate a reflectance spectrum representative of the degradation state of smalt using a *Co* K-edge XANES spectrum measured on the sample. Its application to the XANES spectra of samples SLW1-4, presented in Fig. 4A, provides four simulated reflectance spectra shown in Fig. 4B and describes the reflectance properties of the smalt in its current alteration state in the test samples. We observe four spectra with similar features: an intense band centered around 440 nm, a second, less intense band centered around 550 nm, and a final band centered around 615 nm before a sharp increase in reflectance. These characteristics are typical of smalt[33]. However, differences are observed in these simulated spectra, particularly in the intensity of the first band, which decreases as the sample from which the XANES spectrum at the *Co* K-edge was measured has aged for a longer period. This band, centered at 440 nm, is responsible for the blue color of the pigment. These

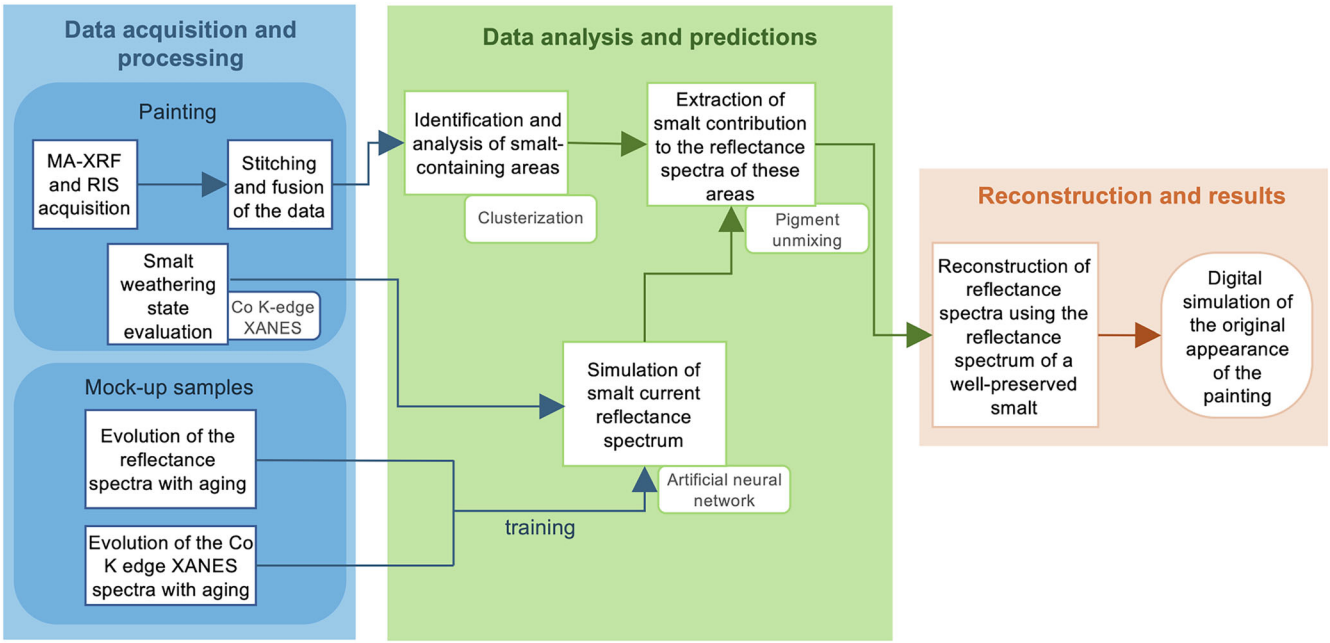

Fig. 3 | Scheme of the developed procedure for the color simulation of discolored smalt pigment in a painting.

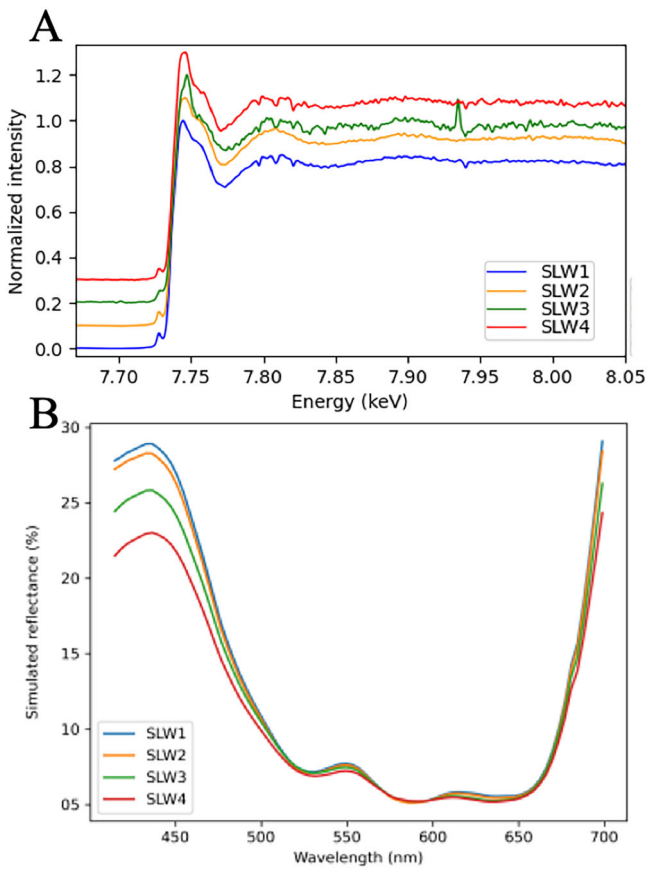

Fig. 4 | Results of characterization and simulation of the smalt pigment in the test samples (SLW1-4). A Mean *Co* K-edge XANES spectra measured. **B** Simulated reflectance spectra of the smalt in its current state in the test samples generated with the Co K-edge XANES spectra using a NN.

observations correspond well to the loss of pigment color as a function of the degradation state.

On the basis of these simulations of smalt reflectance spectra in their respective alteration states, a pigment unmixing can be performed on the reflectance spectra of the test samples containing also lead white. Although the spectral contribution of lead white is expected to remain constant, it increases at the expense of smalt as the sample becomes more degraded (Table 2).

For evaluating the efficieny of the color simulation approach on the test samples, the experimental reflectance spectra of the aged and unaged samples (SLW4 and SLW0, Fig. 5A, B, respectively) are compared to the color reconstruction results (Fig. 5C) using the following procedure. For reconstructing the original color, the key step is that the reflectance spectrum of a well-preserved smalt replaces the simulated one, characteristic of the smalt in its state of preservation, used during the pigment unmixing. The reconstructed spectrum of the test sample is corresponding to the remixed spectrum by summing the reflectance spectra of the two pigments (well-preserved smalt and lead white), weighted by their spectral contributions (Supplementary Figures 19–21).

The simulation results for the SLW4 sample show reconstructed reflectance spectrum, which, compared to the reflectance spectrum of the unaged test sample SLW0, shows many similarities (Fig. 5B, C). The overall intensity of the reconstructed spectrum is slightly overestimated, probably due to the overestimation of the lead white spectral fraction in the deconvolution, which explains that the reconstructed color is brighter than that of the unaged sample. Furthermore, the slope between 470 and 650 nm is slightly more abrupt in the reconstructed spectrum. This explains the purplish hue of the reconstructed color. The L*a*b* values calculated for the reconstructed colors of each aged sample show that the red contribution is overestimated each time, as the a* values range between 7 and 9 (Table 2), whereas the a* value of the unaged sample color is 4.68. However, it is noteworthy that the simulations restore the blue contribution. Indeed, the b* values for the estimated colors are closer to those calculated for the non-aged sample than the experimental values.

The color change expressed as ΔE value was calculated for each simulation test to compare the color of the simulations with the color of the

Table 2 | Spectral contribution of pigments contained in the test samples derived from the pigment unmixing, L*a*b* values calculated on simulated reflectance spectra of test samples in its estimated original color and color differences (Δ*E* see Supplementary Note 1) calculated between the L*a*b* values of the unaged sample SLW0 and those obtained by the color simulation of the aged one

test sample	smalt's contribution	lead white's contribution	L*	a*	b*	Δ*E*
SLW0	0.10	0.90	64.68	4.68	−13.73	–
SLW1	0.12	0.88	65.39	7.00	−17.16	5.41
SLW2	0.13	0.87	64.51	7.16	−17.97	5.15
SLW4	0.25	0.75	57.15	8.63	−24.05	10.31
SLW3	0.14	0.86	63.88	7.26	−18.54	5.11

The L*a*b* values of the unaged sample SLW0 are experimental values of the test sample (see Supplementary Table 1).

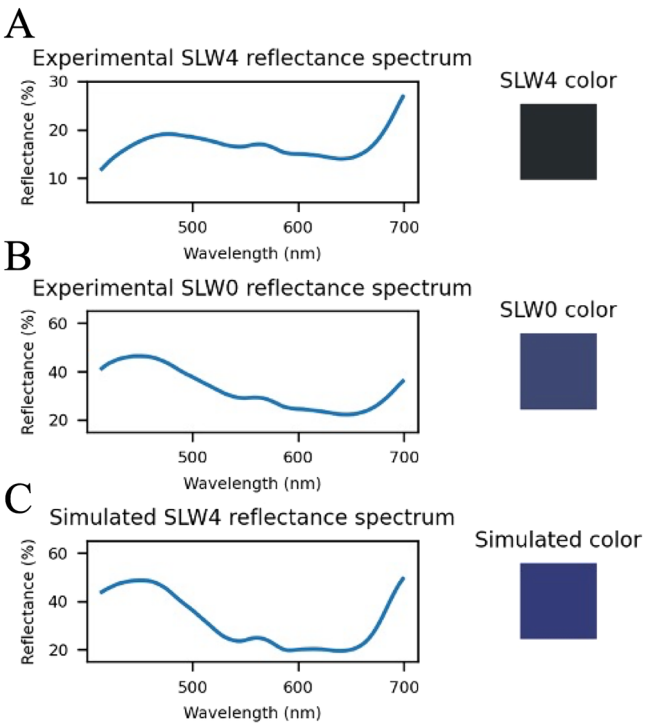

Fig. 5 | Comparison of experimental and simulated reflectance spectra with corresponding color for the test samples. A The experimental reflectance spectrum of the aged test sample SLW4 with the corresponding color. **B** The experimental reflectance spectrum of the unaged test sample SLW0 with the corresponding color. **C** The reconstructed reflectance spectrum of the aged test sample SLW4 with the corresponding simulated original color.

unaged sample (Table 2, see Supplementary Note 1). In this case, the Δ*E* values for SLW1, SLW2, and SLW3 are relatively low (5.41, 5.15, and 5.11, respectively), suggesting that the simulated colors are still distinguishable to the human eye compared to the unaged reference but represent a reasonably accurate reconstruction. However, for SLW4, the value Δ*E* is markedly higher (10.31), indicating a more pronounced deviation from the reference color. This more significant discrepancy could be attributed to the higher proportion of smalt contribution in SLW4, which significantly impacts the overall hue. Despite this, the restoration of the blue contribution in the b* values highlights the strength of the simulation in capturing critical aspects of the aged pigment appearance.

Application to a historical painting: *Abbey among Oak Trees* by Caspar David Friedrich

The investigation of the *Abbey among Oak Trees* (Fig. 6A), which was restored between 2013 and 2016[34,35], was carried out in the museum using the portable SPECIM IQ camera of TU Delft for RIS (Fig. 6B, D) and the equipment developed at the C2RMF[27] for MA-XRF mapping (Fig. 6C).

Alongside stratigraphic cross-sections were collected at specific locations (Fig. 6A) and analyzed using SEM-EDX at the C2RMF (Supplementary Figures 22–26, Supplementary Tables 2–7). XANES profiles were recorded at the *Co* K-edge on the PUMA beamline at SOLEIL and ID21 at ESRF (Fig. 7E). The elemental maps obtained by MA-XRF (Fig. 6C) show that the distributions of *Fe*, *Co*, *K*, and *Ni* are very similar. As these elements are constituents of smalt, it appears that this pigment was widely used in the painting. Smalt is highly present in the sky at the top left, in the trees, in the abbey ruins, and on the ground. However, a slight difference is observed between the *Co* and *K* distributions, particularly in the trees, where the *Co* contribution appears notably higher than that of *K*, suggesting variations in the pigment composition or its degradation behavior in these areas. SEM-EDX analyses of the cross-sections confirmed the presence of smalt in various areas of the artwork. Micrograph of cross-section no. 2 from the sky (Fig. 6F) and chemical maps of this cross-section (Fig. 6G) show the stratigraphy as follows: a red preparation layer composed of aluminosilicate and iron oxides followed by several yellow/grey layers mainly composed of lead white and containing aluminosilicates, *Fe* oxides, vermilion grains, and Ca-rich grains. Finally, the layer closest to the surface predominantly comprises smalt grains, with a few vermilion grains also present. The average composition of smalt grains (Supplementary Tables 2–8) shows that these grains have a composition consistent with the reported compositions of historical smalt used in paintings, particularly regarding their *Co* content, which is around 3%wt[7,36,37]. However, the average *K* content in the grains, which is 4.9%wt, is relatively low. The leaching of K^+ ions from the pigment through ion exchange with the protons in the binder is responsible for the color loss in smalt[12]. This low average *K* content could indicate that the smalt present in the painting has undergone alteration. The leaching of K^+ ions from smalt grains leads to reorganizations within the glassy matrix, creating charge defects around the Co^{2+} ions responsible for the blue color of the pigment. Consequently, the Co^{2+} ions change their coordination from a tetrahedral to a colorless octahedral coordination[21]. Fig. 6E shows the average *Co* K-edge XANES spectrum of the spectra measured on the cross-sections compared to a reference smalt spectrum. The intensity of the pre-peak around 7.3 keV is weaker for the average spectrum measured on the cross-sections of the painting, while the white line around 7.4 keV is more intense and sharper than in the reference spectrum. Additionally, the oscillation around 7.8 keV is lower in energy in the spectrum of the painting compared to the reference. These differences indicate a change in the coordination of Co^{2+} ions from tetrahedral to octahedral. Thus, the XANES spectra measured on the painting confirm that the smalt within the painting is altered. It is also noted that the average XANES spectrum measured on the painting does not match that of fully octahedrally coordinated Co^{2+} ions, indicating that the smalt is in an intermediate state of degradation. While it is recognized that artists such as Rembrandt employed different smalts for various purposes[38], potentially leading to compositional and color variations, the choice of Deffner & Johann smalt reference in our study was driven by practical considerations.

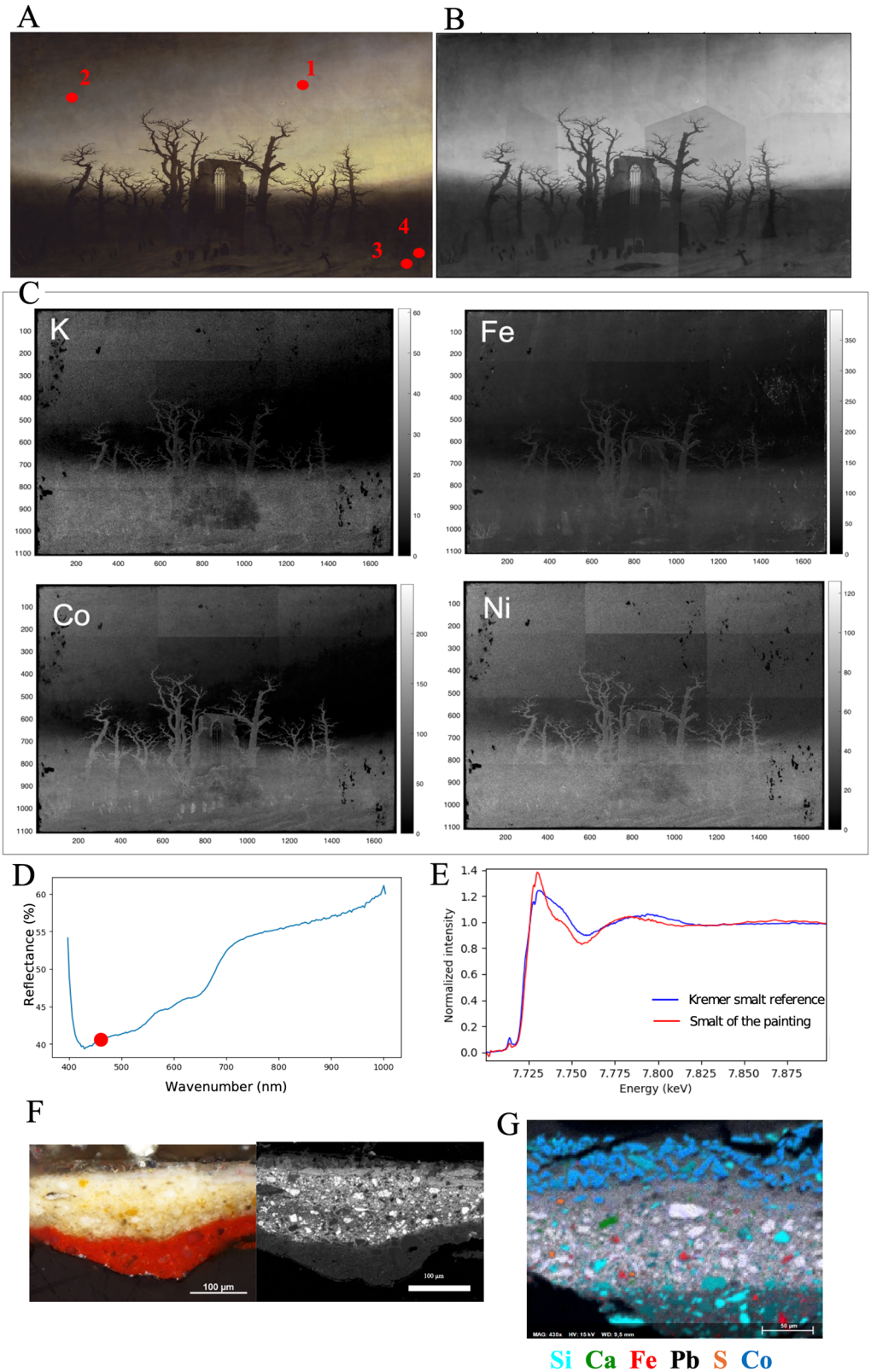

Fig. 6 | Multi-technique analysis of the painting *Abbey among Oak Trees* by Caspar David Friedrich (171 × 110.4 *cm*^{2}, inv. no. NG 8/85, Alte Nationalgalerie, Staatliche Museen zu Berlin-Stiftung Preußischer Kulturbesitz). A Optical image of the painting indicating the positions (1-4) where micro-samples were taken. **B** RIS image of the painting at 450 nm. **C** MA-XRF elemental distribution maps of *K*, *Fe*, *Co*, and *Ni*. **D** Mean reflectance spectrum of the RIS image of the painting, the red dot indicates the wavelength selected to extract the image depicted in (**B**). **E** *Co* K-edge μ-XANES spectra comparing the smalt from the painting (red line) with a Kremer reference (blue line). **F** Cross-section analysis of micro-sample 2: Left image: Optical micrograph under white light. Right image: SEM backscattered electron micrograph. **G** SEM-EDX elemental distribution maps.

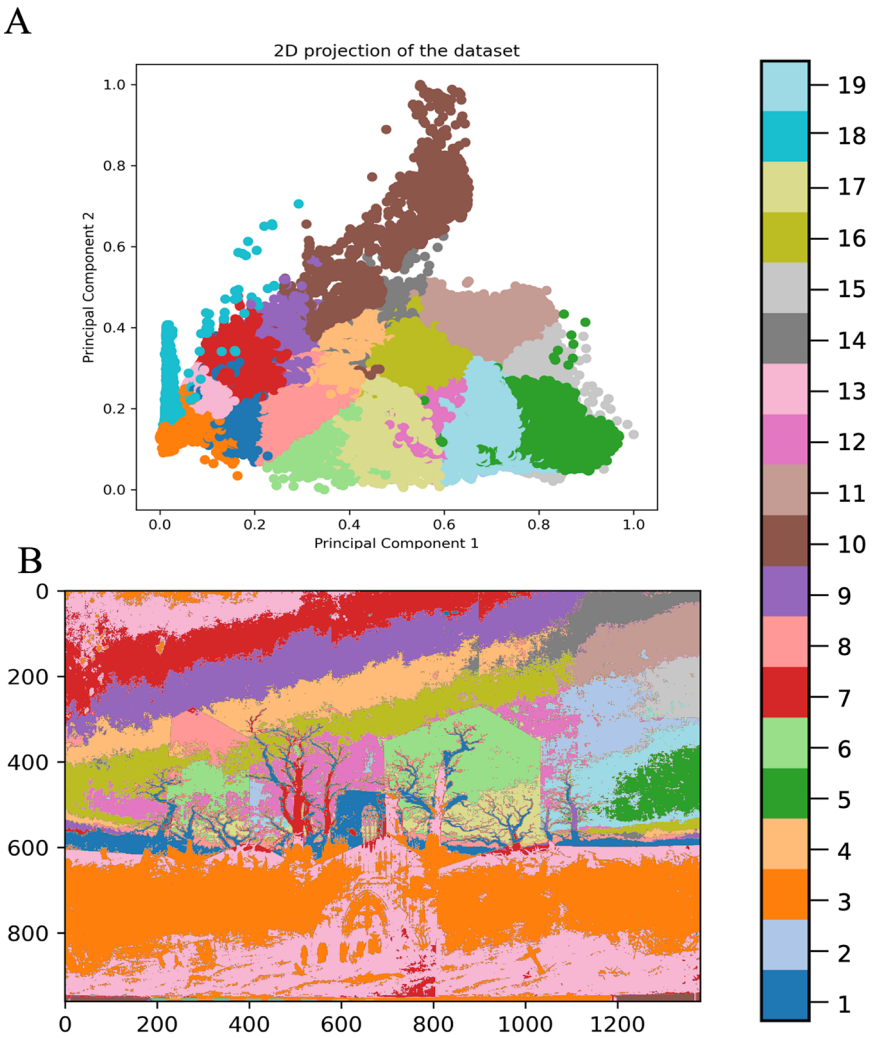

Fig. 7 | Results of clusterization. A 3D PCA plot colorized by the clusterization results. **B** Spatial distribution of the identified clusters across the painting *Abbey among Oak Trees*.

As illustrated above, paintings are far more complex systems compared to model samples. The inhomogeneous mixture of pigments in paint layers, combined with the binding media that contribute to the visual appearance of the painting, necessitates working by zones. A clustering approach was implemented to define these zones. This approach was chosen not only to group areas with similar chemical compositions and colorimetric aspects but also to significantly reduce calculation time and precisely eliminate the need to determine pigment composition on a pixel-by-pixel basis. The clustering was performed using a dataset from the fusion of XRF and RIS mappings to account for the chemical composition and visual aspects. This dataset was first reduced using PCA[39]. The transformed dataset was then clustered using the k-means method[40,41]. The number of clusters was determined by analyzing the silhouette score available in the Supplementary Fig. 27 in the Supplementary Note 2. This analysis allowed us to balance maintaining a sufficient number of clusters to preserve image resolution while ensuring good clustering quality. Based on this compromise, nineteen clusters were chosen. The projection of the data set and the clustering results are shown in Fig. 7A. The clustering yields satisfying results, as most of the painting features are recognizable in the cluster distribution map (Fig. 7B) such as the shading of the sky, the ruins of the abbey, the trees and the monk procession.

In the next step, it is necessary to identify the pigments for each previously defined cluster. The identification is based on the analysis of the mean XRF spectrum of the cluster and the SEM-EDX analysis of the painting cross-section. Taking the example of cluster 1, its mean XRF spectrum (Fig. 8A) shows the presence of various elements, including *S*, *K*, *Ca*, *Fe*, *Co*, *Ni*, *Hg*, and *Pb*. The combination of *K*, *Fe*, *Co*, and *Ni* is indicative of the presence of smalt, *Hg*, and *S*, which can indicate the presence of vermilion, and *Pb*, which can indicate the presence of lead white. The study of cross-sections, such as the one shown in Fig. 6F, G, reveals the presence of a paint layer primarily containing grains composed of *Si*, *Co*, *Ni*, *As*, *Fe*, and *K*, confirming the presence of smalt. Additionally, grains are composed of *S* and *Hg* as well as others containing *Pb* were identified confirming the presence of vermilion and lead white. Other grains, which are rich in *Fe*, indicate the presence of ochre in the painting. These analyses identified smalt, lead white, vermilion, and ochre as the principal pigments in cluster 1. The reflectance spectrum of the altered smalt of the painting is simulated employing the ANN, and the mean spectrum of *Co* K-edge XANES spectra is measured on the corresponding cross-section taken from the painting (Fig. 6E). The simulation displays a reflectance spectrum with a shape characteristic of the smalt reflectance spectrum (Fig. 8B) close to the one simulated for the test sample SLW4. Both spectra show a maximum intensity of 22% for the band centered around 440 nm. Given the determined state of degradation of smalt in the painting, this result is consistent.

The results of the cluster 1 RIS pigment unmixing show that the color of this cluster appears to be dominated by lead white, with a spectral contribution of 74%. Smalt, vermilion, and yellow ochres contribute less, with spectral contributions of 7%, 9%, and 10%, respectively. The remixing of the spectrum by taking these spectral contributions into account and replacing the simulated reflectance spectrum of degraded smalt with the well-preserved one shows a change in the appearance of the reflectance spectrum. Comparing the estimated reflectance spectrum to the experimental one (Fig. 8C, D), it is evident that the overall trends of both spectra are closely

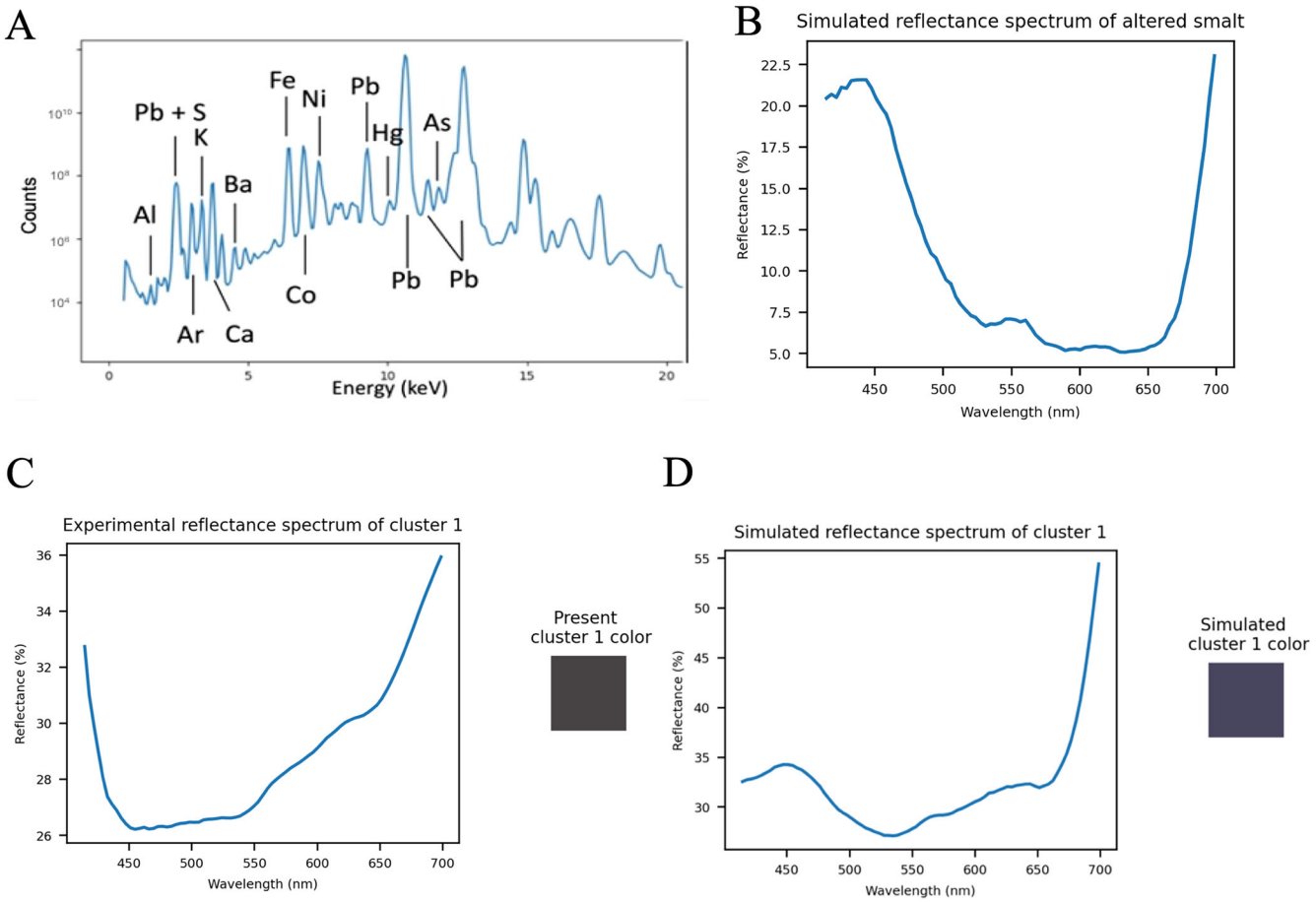

Fig. 8 | A X-ray fluorescence spectrum of the cluster 1 with main elements indicated. **B** Artificial NN simulated reflectance spectrum of altered smalt in the painting. **C** Experimental reflectance spectrum of cluster 1 with the corresponding color. **D** Simulated reflectance spectrum of cluster 1 with the corresponding color.

Fig. 9 | Comparison between a photograph of the painting *Abbey Among Oak Trees* by Caspar David Friedrich (171 × 110.4 cm^2, inv. no. NG 8/85, Alte Nationalgalerie, Staatliche Museen zu Berlin) and the color simulation results. Left: photograph of the painting after restoration in 2016 ©Staatliche Museen zu Berlin, Nationalgalerie / Foto: Kristina Mösl, Francesca Schneider. Right: color simulation image ©Clément de Mecquenem / Lab-BC.

aligned. Both spectra increase towards 700 nm, with reflectance values ranging from 0.45 to 0.63. The contribution of smalt is notable, particularly indicated by the band at 440 nm in the simulated spectrum, even though its intensity is low. However, minor discrepancies, particularly in the region between 500 and 600 nm, suggest potential areas for refinement in the unmixing and remixing model or of the individual spectra of the pigments used.

The color swatches derived from both spectra show a noticeable hue change. The estimated color appears to be cooler and bluer than the measured one. By applying an analogous method to all other clusters containing

deteriorated smalt (Supplementary Figures 28–46), a schematic representation of the painting *Abbey among Oak Trees* can be simulated as depicted in Fig. 9 on the right hand side compared to a photograph of the painting after restoration shown on the left hand side.

Discussion

The comparison between the photograph after the restoration of the painting and the simulated image reveals noticeable color changes in the painting due to aging. The simulated image presents a cooler and more vibrant overall hue, with specific areas exhibiting a more pronounced blue tone. It is consistent to observe that the areas appearing the bluest in the simulated image correspond to regions that contain most of the smalt, according to the chemical analysis presented earlier in the article. This consistency supports the validity of our simulation approach, which provides a new representation of the artwork that could be closer to the initial appearance of the painting before the smalt altered over time. While the developed methodology demonstrates significant promise in simulating the original appearance of degraded smalt pigments, certain limitations must be addressed to improve its accuracy and generalizability. A primary constraint is the dataset used to train the ANN. The training data, comprising 191 Co K-edge XANES spectra and corresponding reflectance spectra, represents a limited range of smalt degradation states. This partial representation constrains the ANN's ability to accurately predict reflectance spectra across the full spectrum of smalt degradation observed in historical paintings. For instance, the current data set does not encompass highly degraded smalt, which is common in many artworks. Furthermore, the relatively small size of the training dataset increases the risk of overfitting during the training process. With 191 Co K-edge XANES spectra and their corresponding reflectance spectra, the ANN may learn noise or specific patterns that do not generalize well to unseen data. This can lead to overly optimistic performance on the training set while reducing the predictive accuracy of the model when applied to smalt pigments with degradation states not represented in the data set. To mitigate this problem, future work should focus on expanding the data set to include a wider range of degradation states and employing regularization techniques or data enhancement strategies to improve the robustness and generalizability of the model. Simpler models based on linear regression could also be tested and compared to the trained ANN model.

A second challenge arises from the variability in historical smalt compositions. Smalt production methods varied significantly across regions and time periods, leading to differences in Co concentrations, alkali content, and impurities like Fe or As. These compositional differences directly impact smalt's optical and chemical properties and its degradation behavior. The Deffner & Johann smalt used in this study provides a practical and accessible modern reference but may not accurately represent the diversity of smalt found in historical artworks. This discrepancy could introduce errors in the simulated reflectance spectra and, by extension, the reconstructed color profiles.

Third, the nature of the binder used by the artist can play a significant role in the optical properties and aging of smalt-containing paint layers. In this study, we did not account for the potential influence of the binder. The use of mock-up samples introduces additional complexities. While these samples are valuable for controlled experimentation, they lack historical paint layers' structural and material heterogeneity. Factors such as particle size, binder composition, and layer stratigraphy significantly influence the reflectance spectra of smalt and other pigments. These parameters were not explicitly considered in the current study, which can limit the accuracy of the simulations when applied to complex historical paintings.

To summarize we developed a robust procedure to simulate the initial color of paintings affected by the alteration of smalt. Applying the procedure to test samples and Caspar David Friedrich's *Abbey Among Oak Trees* provides a compelling proof of concept. The simulated color profile, characterized by cooler and more vibrant hues, is consistent with historical accounts of the original appearance of the smalt. Integrating advanced analytical techniques such as MA-XRF mapping, RIS, and XANES applied to artificially aged model samples and the original painting, combined with ML methods such as ANN, enabled the identification of the painting composition and simulation of the painting with undeteriorated smalt. The reconstructed image of the painting revealed cooler and more vibrant hues, offering a closer approximation of the initial appearance of the painting. While our approach has proven effective, several areas for improvement remain. Eventually, this innovative approach provides a valuable tool for art conservators, allowing for improved informed decisions for the conservation of historical artworks and improving our understanding of artworks and contexts in which they were created. In a more general way, the presented procedure can be adapted to other cases of degraded pigments in artworks.

Data availability

The authors declare that the data supporting the findings of this study are available within the paper and its Supplementary Information files. Raw data files and the Python code used for the simulation can be provided by the corresponding author upon reasonable request.

Received: 5 November 2024; Accepted: 14 July 2025;
Published online: 06 August 2025

References

1. van Loon, A., Noble, P. & Burnstock, A. Ageing and deterioration of traditional oil and tempera paints. In *Conservation of easel paintings*, Routledge series in conservation and museology, 216–243 (Routledge, 2020).
2. De Keyser, N. et al. Reviving degraded colors of yellow flowers in 17th century still life paintings with macro- and microscale chemical imaging. *Sci. Adv.* **8**, eabn6344 (2022).
3. Dik, J. et al. Visualization of a Lost Painting by Vincent van Gogh Using Synchrotron Radiation Based X-ray Fluorescence Elemental Mapping. *Anal. Chem.* **80**, 6436–6442 (2008).
4. Monico, L. et al. Degradation Process of Lead Chromate in Paintings by Vincent van Gogh Studied by Means of Synchrotron X-ray Spectromicroscopy and Related Methods. 1. Artificially Aged Model Samples. *Anal. Chem.* **83**, 1214–1223 (2011).
5. Miliani, C. et al. Photochemistry of Artists' Dyes and Pigments: Towards Better Understanding and Prevention of Colour Change in Works of Art. *Angew. Chem. Int. Ed.* **57**, 7324–7334 (2018).
6. De La Rie, E. R. Old master paintings: a study of the varnish problem. *Anal. Chem.* **61**, 1228A–1240A (1989).
7. Delamare, F. Aux origines des bleus de cobalt : les débuts de la fabrication du saffre et du smalt en Europe occidentale. *Comptesrendus des. s.éances de. l ann.ée - Acad.émie des. Inscr. et. belles-Lett.* **153**, 297–315 (2009).
8. Stege, H. Out of the blue?. *Z. für. Kunsttechnol.* **18**, 121–142 (2004).
9. Mühlethaler, B. & Thissen, J. SMALT. *Stud. Conserv*. **14**, 47–61 (1969).
10. Cianchetta, I. et al. Discoloration of the smalt pigment: experimental studies and ab initio calculations. *J. Anal. At. Spectrom.* **27**, 1941 (2012).
11. Spring, M., Higgitt, C. & Saunders, D. Investigation of Pigment-Medium Interaction Processes in Oil Paint containing Degraded Smalt. *Natl Gallery Tech. Bull.* **26**, 56–70 (2005).
12. Robinet, L., Spring, M. & Pag,s-Camagna, S. Vibrational spectroscopy correlated with elemental analysis for the investigationof smalt pigment and its alteration in paintings. *Anal. Methods* **5**, 4628 (2013).
13. De Mecquenem, C. et al. Influence of the painting medium on the alteration process of smalt in oil paintings studied using combined K and Co K-edge XANES. *Appl. Phys. A* **130**, 781 (2024).
14. Langle, S. B. L'Éloge du doute en Restauration des œuvres d'art. *CeROArt* http://journals.openedition.org/ceroart/4627 (2015).
15. Parvathaneni, T. S. R., Pisarenco, M. & Onvlee, H. A Deep Learning Approach for Digital Color Reconstruction of Van Gogh's Paintings Using Unpaired Areas Under the Frame. *SN Computer Sci.* **5**, 498 (2024).

16. Mol, V. R. & Maheswari, P. U. The digital reconstruction of degraded ancient temple murals using dynamic mask generation and an extended exemplar-based region-filling algorithm. *Herit. Sci.* **9**, 1–18 (2021).
17. Van Loon, A. et al. The role of smalt in complex pigment mixtures in Rembrandt's Homer 1663: combining MA-XRF imaging, microanalysis, paint reconstructions and OCT. *Herit. Sci.* **8**, 90 (2020).
18. Carter, J., van Loon, A., Keune, K. & Froment, E. From purple to brown: Using degradation products in reconstructions of a complex smalt paint mixture in The Night Watch to study color change. In *Working Towards a Sustainable Past*. ed. J. Bridgland, Valencia (2023).
19. Geldof, M., Proaño Gaibor, A. N., Ligterink, F., Hendriks, E. & Kirchner, E. Reconstructing Van Gogh's palette to determine the optical characteristics of his paints. *Herit. Sci.* **6**, 1–20 (2018).
20. Biever, C. St Luke's new coat. *Nature* **417**, 219–220 (2002).
21. Robinet, L., Spring, M., Pagés-Camagna, S., Vantelon, D. & Trcera, N. Investigation of the Discoloration of Smalt Pigment in Historic Paintings by Micro-X-ray Absorption Spectroscopy at the Co K-Edge. *Anal. Chem.* **83**, 5145–5152 (2011).
22. Cotte, M. et al. The ID21 X-ray and infrared microscopy beamline at the ESRF: status and recent applications to artistic materials. *J. Anal. At. Spectrom.* **32**, 477–493 (2017).
23. Salomé, M. et al. The ID21 Scanning X-ray Microscope at ESRF. *J. Phys.: Conf. Ser.* **425**, 182004 (2013).
24. Tack, P. et al. Investigation of (micro-)meteoritic materials at the new hard X-ray imaging PUMA beamline for heritage sciences. *J. Synchrotron Radiat.* **26**, 2033–2039 (2019).
25. Schöder, S. Heritage research at the PUMA beamline. *Appl. Phys. A* **130**, 911 (2024).
26. Solé, V., Papillon, E., Cotte, M., Walter, P. & Susini, J. A multiplatform code for the analysis of energy-dispersive X-ray fluorescence spectra. *Spectrochimica Acta Part B: At. Spectrosc.* **62**, 63–68 (2007).
27. Ravaud, E. et al. Development of a versatile XRF scanner for the elemental imaging of paintworks. *Appl. Phys. A* **122**, 17 (2016).
28. Alfeld, Matthias. DataHandlerP. DataHandlerP, https://sourceforge.net/projects/datahandlerp/.
29. Pillay, R., Hardeberg, J. Y. & George, S. Hyperspectral imaging of art: Acquisition and calibration workflows. *J. Am. Inst. Conserv.* **58**, 3–15 (2019).
30. Duncan, D. R. The colour of pigment mixtures. *Proc. Phys. Soc.* **52**, 390–401 (1940).
31. Kubelka, P. & Munk, F. Ein Beitrag zur Optik der Farbanstriche. *Z. tech. Phys.* **12**, 593–601 (1931).
32. Kubelka, P. New Contributions to the Optics of Intensely Light-Scattering Materials. *Part I. JOSA* **38**, 448–457 (1948).
33. Van Der Weerd, J., Van Veen, M. K., Heeren, R. M. A. & Boon, J. J. Identification of Pigments in Paint Cross Sections by Reflection Visible Light Imaging Microspectroscopy. *Anal. Chem.* **75**, 716–722 (2003).
34. Mösl, K.. *Mönch am Meer und Abtei im Eichwald. Forschungen zur Maltechnik Caspar David Friedrichs*. Ph.D. thesis, Univerity of Fine Arts Dresden, Dresden (2021).
35. Mösl, K. & Demandt, P. (eds) *Der Mönch ist zurück. Die Restaurierung von Caspar David Friedrichs Mönch am Meer und Abtei im Eichwald,* Nationalgalerie, Staatliche Museen zu Berlin, 32p. (2017).
36. Zlámalová Cílová, Z., Gelnar, M. & Randáková, S. Smalt production in the Ore Mountains: Characterization of samples related to the production of blue pigment in Bohemia. *Archaeometry* **62**, 1202–1215 (2020).
37. Gratuze, B., Soulier, I., Barrandon, J. & Foy, D. De l'origine du cobalt dans les verres. *Rev. d'Archéométrie* **16**, 97–108 (1992).
38. Janssens, K. et al. Rembrandt's 'Saul and David' (c. 1652): Use of multiple types of smalt evidenced by means of non-destructive imaging. *Microchemical J.* **126**, 515–523 (2016).
39. Abdi, H. & Williams, L. J. Principal component analysis. *WIREs Computational Stat.* **2**, 433–459 (2010).
40. Lloyd, S. Least squares quantization in PCM. *IEEE Trans. Inf. Theory* **28**, 129–137 (1982).
41. Arthur, D. & Vassilvitskii, S. K-Means++: The Advantages of Careful Seeding, In: *Proceedings of the 18th Annual ACM-SIAM Symposium on Discrete Algorithms, New Orleans* **8**, 027–1035 (2007).

Acknowledgements

We gratefully thank Ralph Gleis, Birgit Verwiebe, and Kerstin Krainer, formerly Alte Nationalgalerie, Staatliche Museen zu Berlin (ANG), for this study's fruitful cooperation and long-lasting support. The staff of the ANG was thanked for their support during day and night analytical shifts in the museum. This work was supported by the Aldried Krupp von Bohlen und Halbach-Stiftung Foundation. This work was also supported by the University School of Humanities, Creation, Heritage, Investment of Future ANR-17-EURE-0021 – Fondation des Sciences du Patrimoine (FSP) through the MARCS project. We especially acknowledge Vincent Detalle† and Emmanuel Poirault for supporting the transportation of the equipment to the ANG by providing the FSP transporter. We want to thank the SOLEIL synchrotron facility and Sebastian Schöder and Laurent Tranchant for their support during measurements at the PUMA beamline (Proposal ID 20220455). We would also like to acknowledge the ESRF synchrotron facility for providing beamtime at the ID21 beamline and Marine Cotte for her help (Proposals HG157 and HG211).

Author contributions

Conceptualization: I.R., M.E., K.M., C.M.; Methodology: C.M., M.E., I.R., M.A., T.C.; Investigation: C.M., M.E., M.A., T.C., E.L., K.M., I.R.; Data Curation: C.M., M.E., M.A., E.L.; Formal Analysis: C.M., M.E., M.A., E.L., I.R.; Software: C.M., M.A.; Visualization: C.M.; Supervision: I.R., M.E., M.A.; Writing—original draft: C.M., M.E., I.R.; Writing—review & editing: I.R., M.E., M.A., T.C., K.R.

Competing interests

The authors declare no competing interests.

Additional information

Supplementary information The online version contains supplementary material available at https://doi.org/10.1038/s40494-025-01953-y.

Correspondence and requests for materials should be addressed to Ina Reiche.